The Astrophysical Journal, 806:77 (7pp), 2015 June 10 doi:10.1088/0004-637X/806/1/77

NANODUST DETECTION BETWEEN 1 AND 5 AU USING *CASSINI* WAVE MEASUREMENTS

P. Schippers[1], N. Meyer- Vernet[1], A. Lecacheux[1], S. Belheouane[1], M. Moncuquet[1], W. S. Kurth[2], I. Mann[3], D. G. Mitchell[4], and N. André[5]
[1] LESIA—CNRS—Observatoire de Paris, 5 place Jules Janssen, F-92195 Meudon, France
[2] Department of Physics and Astronomy, University of Iowa, Iowa City, IA, USA
[3] EISCAT Scientific Association, Kiruna, Sweden and Department of Physics Umeå University, Sweden
[4] Applied Physics Laboratory, John Hopkins University, Laurel, MD, USA
[5] IRAP, 9 Avenue du Colonel Roche, F-31028 Toulouse, France
Received 2015 February 25; accepted 2015 April 13; published 2015 June 9

ABSTRACT

The solar system contains solids of all sizes, ranging from kilometer-sized bodies to nano-sized particles. Nanograins have been detected in situ in the Earth's atmosphere, near cometary and giant planet environments, and more recently in the solar wind at 1 AU. The latter nanograins are thought to be formed in the inner solar system dust cloud, mainly through the collisional break-up of larger grains, and are then picked up and accelerated by the magnetized solar wind because of their large charge-to-mass ratio. In the present paper, we analyze the low frequency bursty noise identified in the *Cassini* radio and plasma wave data during the spacecraft cruise phase inside Jupiter's orbit. The magnitude, spectral shape, and waveform of this broadband noise are consistent with the signatures of the nano particles that traveled at solar wind speed and impinged on the spacecraft surface. Nanoparticles were observed whenever the radio instrument was turned on and able to detect them at different heliocentric distances between Earth and Jupiter, suggesting their ubiquitous presence in the heliosphere. We analyzed the radial dependence of the nanodust flux with heliospheric distance and found that it is consistent with the dynamics of nanodust originating from the inner heliosphere and picked up by the solar wind. The contribution of the nanodust produced in the asteroid belt appears to be negligible compared to the trapping region in the inner heliosphere. In contrast, further out, nanodust is mainly produced by the volcanism of active moons such as Io and Enceladus.

Key words: interplanetary medium – Sun: heliosphere

1. INTRODUCTION

Interplanetary space contains dust particles over a large range of sizes. They are released through the activity of comets and moons, and the fragmentation and impacts of asteroids. Until recently the smaller particles detected in the interplanetary dust cloud were several tens of nanometers across. Smaller nanograins were remotely identified in the interstellar medium a long time ago through different mechanisms such as far UV extinction, optical luminescence, and infrared emission. However, such remote detection is not as effective for solar system nanodust mainly because of the weak optical depth (Li & Mann 2012), so in situ detection is preferred. Such grains have peculiar properties due to their very small size. In particular, their large surface to-volume ratio favors the surface exchange reactions with their environment, and their large charge-to-mass ratio allows them to be easily accelerated in large-scale electric fields that occur in planetary magnetospheres (Burns et al. 2001) and/or close to moons (Farrell et al. 2012). But they can also be accelerated by the magnetized solar wind, though on longer timescales (Mann et al. 2007), by a process that is akin to the pickup of freshly produced ions in the solar wind (Luhmann 2003). These nanodust particles are then expelled from the inner heliosphere over large distances (Hamilton et al. 1996; Czechowski & Mann 2010).

Nanograins have so far been detected in situ in cometary environments (Utterback & Kissel 1990), in the solar wind at 1 AU by Meyer-Vernet et al. (2009b) and Schippers et al. (2014), and in the environments of giant planets such as Jupiter and Saturn (Hsu et al. 2012, and references therein). The presence of a reservoir of nanograins at 0.2 AU has been theoretically predicted by Mann et al. (2007) and is suspected to be the main source of nanodust in the inner heliosphere. Indeed, dust is generated by mutual collisions in the solar system dust cloud and the production rate is expected to increase toward the Sun where increasing number density and relative velocities lead to a maximum production of the dust fragments. In the vicinity of the Sun, the interplay of gravity and electromagnetic forces leads to a trapping of the dust and this occurs under certain conditions at approximately 0.2 AU (Czechowski & Mann 2010). In the outer heliosphere, the nanodust sources identified so far are the giant planet moons Io (Maravilla et al. 1995) and Enceladus (Spahn et al. 2006), which are geologically active and release dust through volcanism and cryovolcanism, respectively.

Other than dust analyzers, which are designed to measure the micron-sized grains in situ (Auer 2001), radio wave instruments have the ability to detect dust grains (Oberc 1996). This technique is used in the present paper. It is based on the principle that the high-speed impacts of grains on the spacecraft induce electric pulses that are recorded by the wave receivers (Meyer-Vernet et al. 2015). Meyer-Vernet et al. (2009b) reported the first nanodust detection at 1 AU with the radio instrument on the *Solar Terrestrial Relations Observatory* (*STEREO*). This detection was made possible by the high - speed of these particles, which was near the solar wind speed due to their high charge-to-mass ratio (Mann et al. 2014). More recently, Schippers et al. (2014) confirmed this discovery using the radio measurements of the *Cassini* mission when it flew close to Earth's orbit in 1999 August. The radio and plasma wave instrument (RPWS) on board *Cassini* was episodically turned on during its cruise phase and recorded signatures

similar to those observed by the same instrument when *Cassini* encountered high-speed nanodust near Jupiter (Meyer-Vernet et al. 2009a).

The aim of the present paper is to analyze these signatures and understand the origin of the dust. In Section 2 we recall the method of nanodust detection with radio wave instrumentation. In Section 3, we apply the method to identify the dust and estimate the flux with radio wave data on board *Cassini*. The results are discussed in Section 4.

2. IN SITU DUST DETECTION WITH A RADIO RECEIVER

2.1. Basics of Dust Detection With Wave Measurements

Radio and plasma wave instruments have been traditionally used to measure electromagnetic radiation and to monitor electron bulk properties such as density and temperature through the analysis of electrostatic fluctuations induced by the charged particle thermal motion around the antennas (i.e., thermal noise spectroscopy; Meyer-Vernet 1979). Although radio and plasma wave receivers are not designed for dust measurements, they are capable of revealing the presence of microdust and nanodust (within certain conditions). Indeed, electric antennas are sensitive to dust because the high-speed impact of a dust grain on a spacecraft surface generates a plasma cloud whose expansion creates charge decoupling (Drapatz & Michel 1974). This method is complementary to conventional impact ionization dust detectors, which provide more information per impact, but are limited by the small size of the detectors. In the solar wind the spacecraft is positively charged because of photoelectron emission so that the electrons from the expanding cloud are recollected by the target while the expanding ions induce a potential on the spacecraft and antennas (Meyer-Vernet et al. 2014). This holds until the density of the cloud reaches the density of the ambient plasma, so that the characteristic time of this process satisfies

$$\tau_r \lesssim (3Q/(4\pi en))^{1/3}/v_E, \tag{1}$$

where Q is the charge of the plasma cloud, n is the ambient density, and v_E is the expansion velocity (Meyer-Vernet et al. 2009a, 2009b). The electric signal measured by the antennas can then be used as a diagnosis of the dust. This technique is very sensitive because of the large detection area and solid angle that are the result of the whole spacecraft surface being the target. It was first developed to analyze microdust at Saturn using the radio instrument on board Voyager (Aubier et al. 1983; Gurnett et al. 1983; Meyer-Vernet et al. 1996), and was extended to fast nanodust detection at Jupiter (Meyer-Vernet et al. 2009a) using the wave data from *Cassini*, and at 1 AU using *STEREO*/WAVES (Meyer-Vernet et al. 2009b) and *Cassini*/ RPWS (Schippers et al. 2014).

The maximum voltage amplitude between one antenna and the spacecraft produced by the impact of one dust grain on the spacecraft surface can be written as

$$\delta V \simeq \Gamma Q/C, \tag{2}$$

where Q is the charge generated by the dust impact, C is the capacitance of the spacecraft surface, and Γ is the antenna gain ($\simeq$0.4 in this case). The impact charge Q depends on the grain mass and speed, with various relationships of the form $Q \propto m^{\alpha} v^{\beta}$, with $\alpha \simeq 1$ and $\beta \simeq 3-4.5$. The coefficients depend on mass, speed, angle of incidence, and grain and target composition (Goeller & Gruen 1989; Burchell et al. 1999), and have not been measured for either nanodust or $v > 70$ km s^{-1} (Auer 2001).

According to McBride & McDonnell (1999), the charge released can be approximated by

$$Q = 0.7\, mv^{3.5}, \tag{3}$$

where m and v are respectively the mass and the speed of the grain. This method is then sensitive to massive dust particles and/or fast particles (speeds higher than a few km s^{-1}) as the induced charge is strongly dependent on the speed. However, it is not able to separately determine the speed and the mass of the particles. Note that impact ionization yields of materials relevant for *Cassini* have been reported for microdust at speeds <40 km s^{-1} (Collette et al. 2014). Extrapolating these results for nanodust impacting at several hundreds of km s^{-1} produces charges of the same order of magnitude as Equation (3).

The power spectrum of pulses of amplitude (2) with impact rate unity is

$$V_{fi}^2 \simeq 2(\Gamma Q/C)^2 \omega^{-2}\left(1 + \omega^2 \tau_r^2\right)^{-1}, \tag{4}$$

where τ_r is the pulse rise time and $\tau_d >> 1/\omega$ the pulse decay time (Meyer-Vernet 1985). When the rise time exceeds $1/\omega$, which occurs in low density plasma such as solar wind, the signal is then proportional to

$$V_{fi}^2 \propto \omega^{-4}. \tag{5}$$

For a cumulative distribution of the grain flux $F(m)$ over a surface S, the expected power spectrum is

$$V_f^2 \simeq S \int_{m_{\min}}^{m_{\max}} dm \frac{dF(m)}{dm} V_{fi}^2(m). \tag{6}$$

2.2. Plasma Wave Instrument On Board Cassini

The radio and plasma wave instrument on board *Cassini* (Gurnett et al. 2004) is composed of five detectors that are connected to three 10 m length electric antennas. The present analysis is mainly based on the High Frequency Receiver (HFR), which acquires the power spectral density from 3.7 kHz to 16 MHz (in the present study we only use the lowest filter ranging up to 16 kHz). We also analyze time series measured by the Five-Channel Waveform receiver, which acquires waveforms in passbands of either 1–26 Hz or 3 Hz–2.5 kHz. On *Cassini*, the antennas are positioned symmetrically with respect to the spacecraft body, which means that we expect that the measurement in "monopole" mode (when the potential is measured between one antenna and the spacecraft body) should be similar for all the antennas (Meyer-Vernet et al. 2014). As a consequence, the voltage measured in "dipole" mode (potential difference between two antennas) should be negligible in the absence of other sources of electric fields and of dust impact on one of the antennas. On *Cassini*, one of the antennas is always connected in monopole (w), while the two other antennas are either connected in monopole or dipole (u–v). Thus, in the present study, we will use the absence of a signal in dipole mode to ensure that the data used are not contaminated by plasma and electromagnetic waves, and base the dust measurements on data acquired in monopole mode.

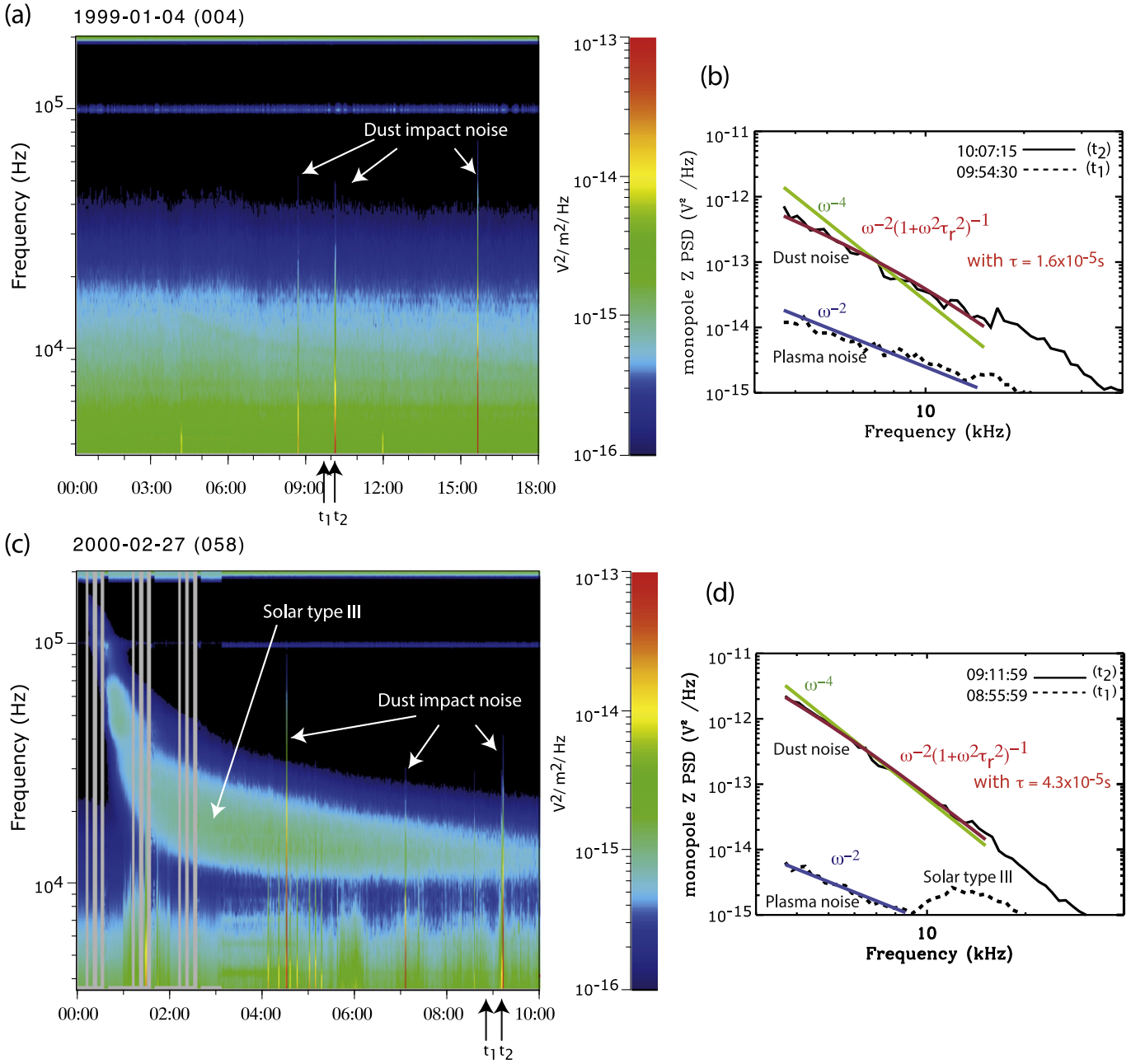

Figure 1. Panel (a): electric power spectral density as a function of frequency and time on day 004 of 1999 between 00:00 and 18:00 UT and acquired with antenna Z in monopole mode. Panel (b): voltage power spectral density spectra at 09:54 UT and 10:07 UT, in solid and dashed lines, respectively. Three power spectral density models are superimposed: (1) the dust impact model $V_f^2 \propto \omega^{-2}(1+\omega^2\tau_r^2)^{-1}$ (in red); (2) the dust impact model with $\tau_r >> 1/\omega$: $V_f^2 \propto \omega^{-4}$ (in green); and (3) the plasma noise model $V_f^2 \propto \omega^{-2}$ (in blue). Panels (c) and (d): same as Panels (a) and (b) on day 058 of 2000 between 00:00 UT and 10:00 UT.

3. DUST IDENTIFICATION AND FLUX CALCULATION

3.1. Wave Data Set

During its phase cruise to Saturn, the instruments on board *Cassini* were turned on several times, which will be discussed in turn below.

3.1.1. The ICO Period: 1.6 AU

From 1998 December to 1999 January, the instruments underwent a commisioning phase ("ICO").

Figure 1(a) displays the electric power density spectrogram in $V^2/m^2/Hz$ acquired by the HFR receiver in monopole mode (w) on 1999 January 4 between 00:00 UT and 18:00 UT, when the spacecraft was at a heliospheric distance of 1.56 AU. We observe (1) a continuous background noise at low frequency - due to the impact of the plasma on the spacecraft and (2) a sporadic and bursty broadband signal. Figure 1(b) shows the voltage power spectral density at two different times on day 1999-004: inside and outside a "burst" event. At 09:54:30 UT (outside), the signal is well-modeled by a power law $\propto \omega^{-2}$, which is typical of a plasma ("shot") noise signature in both amplitude and spectral index (Meyer-Vernet & Perche 1989). At 10:07 UT, the voltage power is enhanced by two orders of magnitude, and the slope is steeper than the plasma background

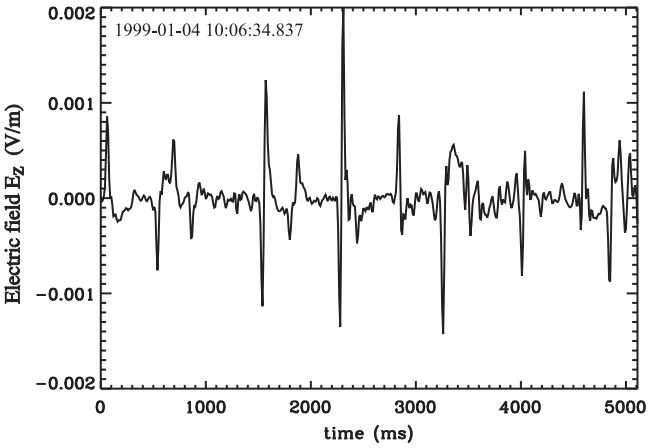

Figure 2. Electric field time series acquired by the RPWS/Waveform receiver (WFR) on 1999 January 4 on monopole w. The signal displays spiky signatures that are typical of nanodust impacts on the spacecraft (Zaslavsky et al. 2012).

noise. We have superimposed two approximate models of the dust impact power spectrum with Equations (4) and (5), respectively in red and green.

Figure 2 displays the electric field time series acquired by WFR in monopole mode the same day, at 10:06:34 UT. We observe the following.

1. The signal displays a series of spikes typical of dust impact ionization. The complicated shape is expected to be produced by the electric field induced by the impact ions, the recollected electrons, and the finite charging timescale of the spacecraft/antenna/receiver system.
2. The amplitude of the electric field in the spike $\delta E = \delta V/L \simeq 1\,\mathrm{mV\,m^{-1}}$ is consistent with the potential (Equation (2)) produced by the impact of particles of a few nanometers at about the solar wind speed (with $L = 10\,\mathrm{m}$, $C = 200\,\mathrm{pF}$, and the induced charge given by Equation (3)).
3. The occurrence of the spikes is consistent with the flux on the spacecraft surface $S \simeq 15\,\mathrm{m^2}$ of interplanetary nanograins predicted by extrapolating the Grün et al. (1993) model to the sub-micron size range using the collisional fragmentation law $F(m) \propto m^{-5/6}$.

3.1.2. Near Earth's Orbit: 1 AU

From 1999 August 15 and September 15, the *Cassini* instruments were turned on during the Earth flyby (1999 September 19). Schippers et al. (2014) reported the first nanodust detection at about 1 AU with *Cassini* using RPWS/HFR data during this period; those results confirmed the *STEREO* observations by Meyer-Vernet et al. (2009b).

3.1.3. In the Asteroid Belt: 2.9 AU

Between 2000 February 23 and March 3, the radio instrument was turned on again. The *Cassini* spacecraft was then around 2.9 AU, within the asteroid belt. Figures 1(c) and (d) display the same information as in Figures 1(a) and (b) for 2000 February 27. In this data sample, we observe the following.

1. The plasma noise level (proportional to the plasma density) is smaller than in Figure 1(b) by a factor of about 3, equal to the the solar wind density decrease between 1.6 and 2.9 AU.
2. The dust noise intensity is extremely variable.
3. The dust noise is closer to the ω^{-4} power-law model. This is consistent with the first point, since the rise time (Equation (1)) is expected to increase as the local plasma density decreases.

3.1.4. Beyond the Asteroid Belt up to Jupiter's Orbit

Before *Cassini* reached its closer position to Jupiter (2000 December 30), the instrument was turned on for about four months. However, during this period the RPWS/HFR mode was not adequate for detecting nanograin impacts because at a closer distance to the planets, the instrument configuration was adapted in order to measure planetary radioemissions at a high rate. To do so, the integration time Δt was set to a value four times smaller than during the previous period. Since the receiver averages the spectral density over the integration time, grain detection requires that the impact rate be high enough to ensure at least one impact during this time.

Unfortunately, Δt then becomes so small that during this period virtually no nanograin can impact the spacecraft surface unless the flux is much greater than the model (black line in Figure 5). Indeed, with a cumulative flux $\propto \mathrm{m}^{-5/6}$, the maximum mass impacting during Δt, given by $F(m_{\max})S\,\Delta t \simeq 1$, is smaller than that of 1 nm grains. A possible explanation for the lack of subnanometer grains is that the electric field at the grain surface becomes so high that the electrostatic stress can exceed the maximum grain cohesion strength, causing the grain's explosion (Meyer-Vernet et al. 2015).

3.2. The High Energy Particle Detector Discharge Issue

During the early mission, the Magnetospheric Imaging Instrument (MIMI; Krimigis et al. 2004) on board *Cassini* reported an issue: discharges of the Imaging Neutral Camera (INCA), possibly triggered by dust impacts and/or sunlight shining on the charged particle rejection plates (Schippers et al. 2014). These discharges were thought to be produced by the negative high voltage applied to the plates. Evidence was found that RPWS data were contaminated by MIMI/INCA discharges (Schippers et al. 2014). A discharge monitor was incorporated in the MIMI instrument to identify and discard the corrupted data. It takes into account a couple of noise indicators that are identifiable in a few control parameters of INCA. Using this device led us to remove short time intervals that were possibly affected by contamination by these discharges. This type of contamination was strongly reduced after the MIMI instrument team decided to turn off the negative voltage mode on day 13 of 2001.

3.3. Nanodust Flux Determination

To calculate the flux of nano particles from the measured power spectral density from Equation (6), we need the following.

1. To assume a power index for the distribution function $F(m)$. Here we choose the low mass extrapolation of the interplanetary dust model by Grün et al. (1985), which

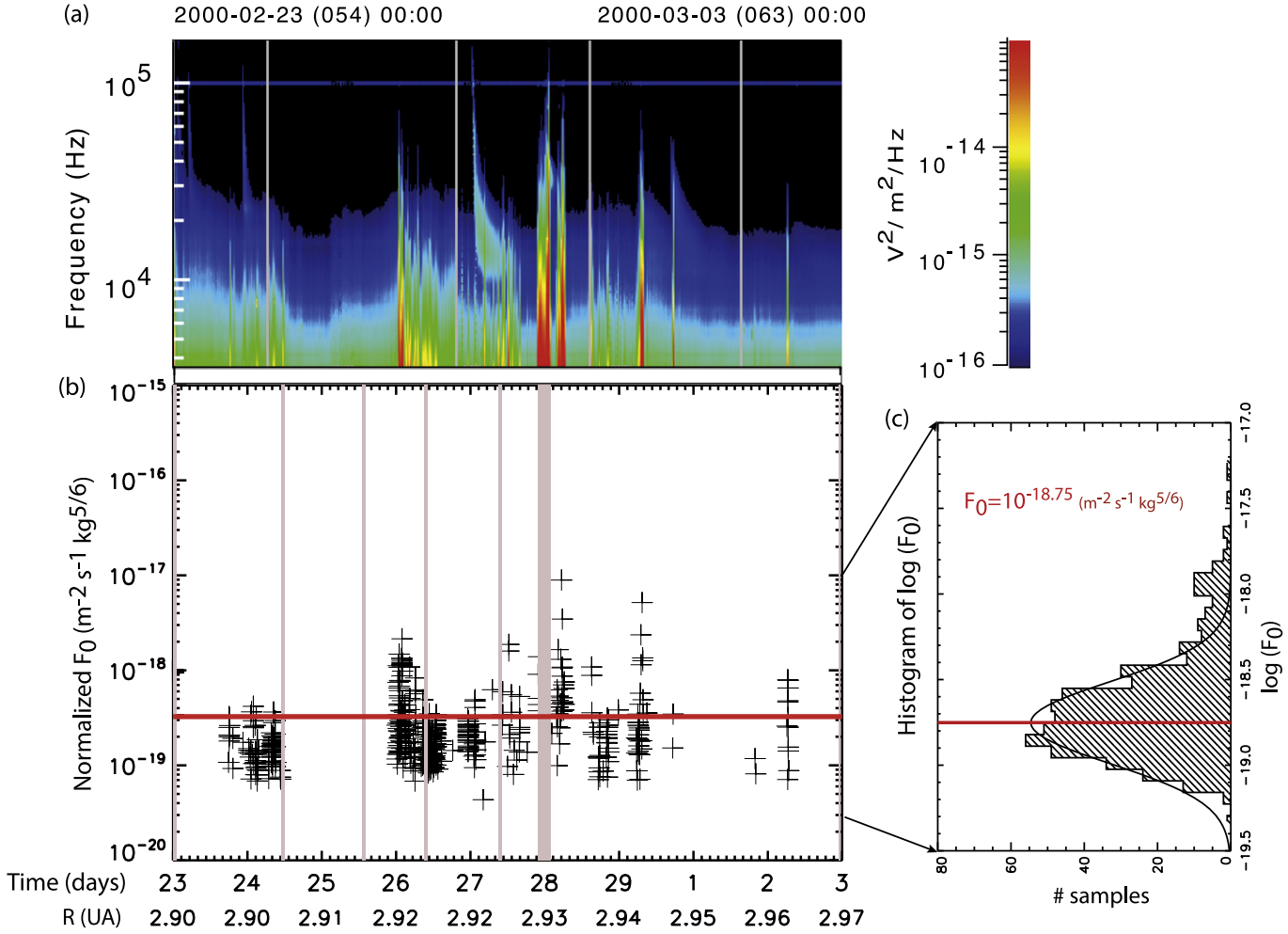

Figure 3. Panel (a): RPWS/HFR spectrogram of the electric field below 200 kHz between 2000 February 23 and March 03. Panel (b): normalized nanodust flux F_0 calculated by equating the theoretical power spectra model expected for a dust mass distribution flux $F = F_0 m^{-5/6}$ from dust collisional fragmentation (Dohnanyi 1969) and the measured power V_f^2 at 10 kHz. Gray vertical lines indicate time intervals when MIMI/INCA discharges were identified (discarded from our data set). Panel (c): Histogram of F_0 for the full time interval.

yields the cumulative distribution

$$F(m) = F_0 m^{-5/6}.$$

In that case, Equations (4) and (6) lead to:

$$V_f^2 \simeq 0.7\, S\left(\Gamma/C\tau_r\right)^2 v^7 F_0 m_{\max}^{7/6}\, /\omega^4,$$

where S is the spacecraft surface ($\simeq$15 m^2), $m_{\min}$ and $m_{\max}$ are the minimum and maximum detected mass in kg, v is the speed in km s^{-1}, and the approximation (5) is valid for $\omega\tau_r \gg 1$.

2. To consider the speed of the grain particles $\boldsymbol{v_d}$. Numerical simulations show that at distances farther than 1 AU, grains with radii smaller than about 10 nm are accelerated at a speed close to

$$\boldsymbol{v_d} = \frac{\left(\boldsymbol{v_{sw}} \times \boldsymbol{B}\right) \times \boldsymbol{B}}{B^2},$$

where $\boldsymbol{v_{sw}}$ is the solar wind speed and $\boldsymbol{B}$ is the interplanetary magnetic field (Czechowski & Mann 2012; Meyer-Vernet et al. 2015). According to Equation (9), we estimate a nanograin impact speed of 360 km s^{-1} at 1.6 AU and 450 km s^{-1} at 2.9 AU.

At each time, we calculate the flux F_0 by equating the expression (8) to the measured spectral power (Schippers et al. 2014). In order to eliminate the contributions of discharges, radio and plasma emissions, and plasma quasi-thermal noise, we have carefully selected the times when the following conditions are met.

1. MIMI/INCA indicators do not show evidence of the presence of discharges (from Section 3.2).
2. The average index of the power law adjusted to the measured spectrum lies between −2.2 and −4, as expected for dust impacts (from Section 2.1).
3. The levels of the three monopoles are similar (within 50%) when they are available (Meyer-Vernet et al. 2009a), as expected for pulses in spacecraft potential.
4. The ratio between the measurements in monopole and dipole mode is greater than a factor of 3. This condition enables us to eliminate contributions from plasma wave electric fields.

The flux calculation and criteria were applied to the data acquired during the *Cassini* ICO period (1999 January 4) and the asteroid belt crossing (2000 February 23–2000 March 3). Figure 3(a) displays the power spectral density for the asteroid belt crossing. The corresponding normalized flux F_0 is plotted

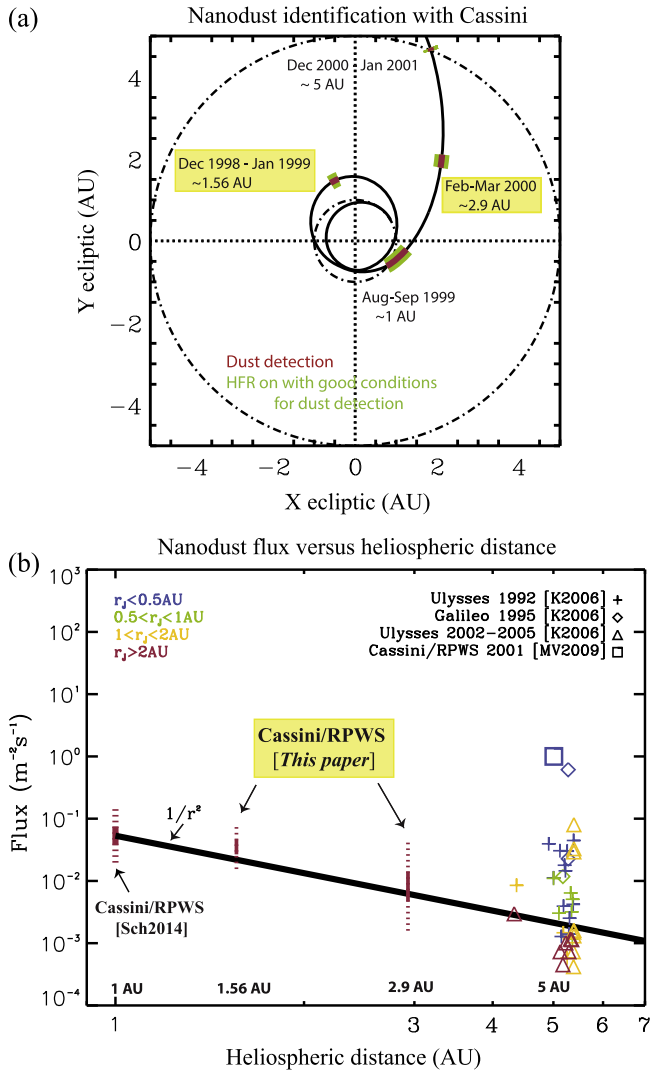

Figure 4. Panel (a): *Cassini* trajectory (black solid line) with periods when the RPWS/HFR detector was able to detect dust (in green) and when we actually observe nanodust (in red). With *Cassini* we were able to identify nanodust whenever the instrument could measure it: after Earth flyby at 1 AU (Schippers et al. 2014; confirmation of *STEREO* results by Meyer-Vernet et al. 2009b), at 1.56 AU (this paper), at 2.9 AU (this paper), and 5 AU (Meyer-Vernet et al. 2009a). Panel (b): radial dependence of nanodust flux with mass $= 10^{-20}$ kg. *Cassini* measurements (except at 5 AU) appear to follow the decreasing trend $\propto \frac{1}{r^2}$ (solid black line) predicted by simulations (see Figure 5). At 5 AU, we superimposed measurements from Krüger et al. (2006) obtained with *Galileo* and *Ulysses*. The references (K2006), (MV2009), and (Sch2014) stand for Krüger et al. (2006), Meyer-Vernet et al. (2009a), and Schippers et al. (2014), respectively.

in Figure 3(b) with black crosses, with the discharge intervals indicated in gray vertical lines. The horizontal line represents the flux F_0 averaged on the whole time interval. Figure 3(c) displays the histogram of the flux values. It shows a Gaussian distribution around $F_0 \simeq 10^{-18.75\pm0.23}\,\mathrm{m^{-2}\,s^{-1}\,kg^{5/6}}$, with a slight excess toward large values. Note the lack of data points in the low flux part of the distribution, which is expected to be due to the threshold effect of the criteria described above and to the small integration time Δt. The average normalized flux calculated from data acquired at 1.6 AU is $F_0 \simeq 10^{-18.12\pm0.11}\,\mathrm{m^{-2}\,s^{-1}\,kg^{5/6}}$, whereas the average normalized flux determined at 1 AU (Schippers et al. 2014) is $F_0 \simeq 10^{-17.94\pm0.14}\,\mathrm{m^{-2}\,s^{-1}\,kg^{5/6}}$.

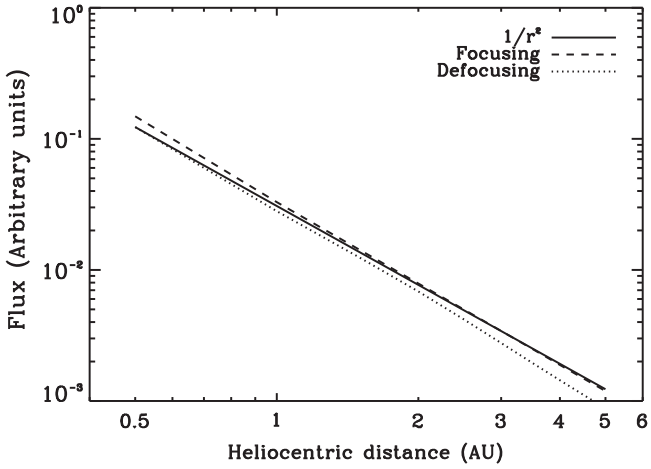

Figure 5. Simulation of nanodust flux distribution across the heliosphere for a dust source located near 0.2 AU, in focusing and defocusing electric field configuration (pointing toward and away from the current sheet, respectively). Dust flux radial dependence is very close to the power law $1/r^2$ (solid line).

4. RADIAL DISTRIBUTION OF NANODUST IN THE HELIOSPHERE AND DISCUSSION

Figure 4 displays the intervals when the instrument was on and able to detect nanodust because the integration time was large enough (marked in green) and displays the intervals when the instrument exhibited nanodust signatures (marked in red). Nanodust is observed whenever the instrument is capable of detecting them.

Our determination of the nanodust flux at three *Cassini* positions (1, 1.6, and 2.9 AU) in the solar wind with *Cassini* gives, for the first time, an estimate of the nano flux radial distribution and hints about the dynamics in the inner heliosphere. In Figure 4, we display the cumulative nanodust flux deduced from the data for particles of mass 10^{-20} kg at the three positions (in red); the solid vertical extension of the bars corresponds to the mean flux value $\pm 1\sigma$ and the dotted bars range from the mean flux $\pm 3\sigma$. The superimposed black solid line represents a r^{-2} power-law model starting from the cumulative flux at 1 AU, F_{1AU}, determined by Schippers et al. (2014) at $m = 10^{-20}$ kg. The other symbols denote measurements close to Jupiter.

The crosses, triangles, and diamonds show data from the Cosmic dust analyzer on board *Ulysses* and *Galileo* (Krüger et al. 2006), whereas the square stems from *Cassini*/RPWS (Meyer-Vernet et al. 2009a). The color code refers to the distance of the spacecraft with respect to Jupiter. These measurements around 5 AU were attributed to high-velocity dust streams ejected by Jupiter (Grün et al. 1993; Grun et al. 1996; Krüger et al. 2006). Various observations by dust detectors on board *Ulysses*, *Galileo,* and *Cassini* during spacecraft encounters with Jupiter together with trajectory simulations (Zook et al. 1996; Graps et al. 2001) have shown a grain size of about 5–10 nm (i.e., mass $\simeq 10^{-21}$–10^{-20} kg) with a speed of 200–450 km s^{-1}.

Our result reveals the following.

1. The nanodust appears ubiquitous in the interplanetary medium at least near the ecliptic between 1 and 5 AU.
2. The interplanetary nanodust flux decreases outward, suggesting production in the innermost heliosphere, inside Earth's orbit, and different from timely and spatially limited sources such as comet and planets. This result is consistent with Mann et al. (2007), who suggested the

existence of a trapping/source region for the nanodust very close to the Sun (0.2 AU) and suggested that this nanodust was picked up and accelerated by the magnetized solar wind (Czechowski & Mann 2010, 2012; Mann & Czechowski 2012).

3. The observations confirm that the interplanetary nanodust flux follows a power-law trend close to r^{-2} outward of 1 AU. This variation was expected since the mean velocity of the particles is expected to change relatively weakly after they have been accelerated close to the solar wind drift velocity, so that the flux conservation yields a decrease in proportion of the inverse squared heliocentric distance. This result is consistent with numerical simulations (Belheouane 2014) of nanodust dynamics. Figure 5 shows the result of numerical simulations of the nanodust dynamics for a source located in the inner heliosphere at 0.2 AU (Mann & Czechowski 2012). The dashed and dotted lines correspond to an inclination of the interplanetary current sheet of 70° (as observed in 1999–2001) for two different polarity orientations of the magnetic field: the dashed line corresponds to a focusing electric field $\boldsymbol{v} \times \boldsymbol{B}$ (i.e., pointing to the heliospheric current sheet) and the dotted line corresponds to a defocusing electric field (i.e., pointing away from the current sheet). We observe that the simulated flux radial dependence is very close to the r^{-2} power-law model displayed with a black solid line.
4. The inner heliospheric source produces the main contribution to the nanodust flux within 5 AU, except very close to Jupiter. The asteroid belt contribution appears to be negligible. Note in particular that *Cassini* was located more than 100° away from the dwarf planet Ceres (Küppers et al. 2014) so we were not able to quantify its production/contribution.
5. Closer than 2 AU from Jupiter, the flux is much higher, corresponding to the nanodust streams of Jovian origin (Zook et al. 1996), the dominant source of nanodust in the planet's vicinity (Graps et al. 2000).

5. CONCLUSION

We analyzed the radio and wave data obtained by *Cassini* from 1997 to 2001 (first part of its cruise phase) to identify nanodust signatures in the interplanetary medium. While the instrument and the operating modes were not designed for this purpose, evidence for nanodust was observed whenever the instrument was turned on with a time integration large enough to enable dust detection. This took place during a few weeks at three different heliospheric distances: 1, 1.6, and 2.9 AU. The observed flux distribution is consistent with nanodust produced in the inner heliosphere as suggested by Mann et al. (2007), picked up by the magnetized solar wind, and filling the heliosphere (Czechowski & Mann 2010, 2012; Mann & Czechowski 2012). This study presents the first results on nanodust detection on a large radial distance range in the interplanetary medium, obtained serendipitously by a single spacecraft during its cruise phase. However, the spatial coverage of the results is limited due to operating modes that were not adapted to the nanodust detection. Incidentally, this shows the importance of the data acquired during mission cruise phases.

The data are from the RPWS/HFR receiver of *Cassini* and are hosted in LESIA, Observatory of Paris. We acknowledge B. Cecconi for his assistance in providing the data. The research at LESIA (Observatory of Paris) is supported by the CNES (Centre National d'Etudes Spatiales) agency. The research at the University of Iowa was supported by NASA through contract 1415150 with the Jet Propulsion Laboratory.

REFERENCES

Aubier, M. G., Meyer-Vernet, N., & Pedersen, B. M. 1983, GeoRL, 10, 5
Auer, S. 2001, in Interplanetary Dust, ed. E. Grün, B. A. S. Gustafson, S. Dermott & H. Fechtig (Berlin: Springer), 385
Belheouane, S. 2014, PhD thesis, Univ. Pierre et Marie Curie
Burchell, M. J., Cole, M. J., McDonnell, J. A. M., & Zarnecki, J. C. 1999, MeScT, 10, 41
Burns, J. A., Hamilton, D. P., & Showalter, M. R. 2001, in Interplanetary Dust, ed. E. Grün, B. A. S. Gustafson, S. Dermott & H. Fechtig (Berlin: Springer), 641
Collette, A., Grün, E., Malaspina, D., & Sternovsky, Z. 2014, JGRA, 119, 6019
Czechowski, A., & Mann, I. 2010, ApJ, 714, 89
Czechowski, A., & Mann, I. 2012, Nanodust in the Solar System: Discoveries and Interpretations (Berlin: Springer-Verlag), 47
Dohnanyi, J. S. 1969, JGR, 74, 2531
Drapatz, S., & Michel, K. W. 1974, ZNatA, 29, 870
Farrell, W. M., Wahlund, J.-E., Morooka, M., et al. 2012, Icar, 219, 498
Goeller, J. R., & Gruen, E. 1989, P&SS, 37, 1197
Graps, A., Grün, E., Svedhem, H., et al. 2001, in Proc. of the Meteoroids 2001 Conference, ed. B. Warmbein (Noordwijk: ESA), 601
Graps, A. L., Grün, E., Svedhem, H., et al. 2000, Natur, 405, 48
Grun, E., Hamilton, D. P., Riemann, R., et al. 1996, Sci, 274, 399
Grün, E., Zook, H. A., Baguhl, M., et al. 1993, Natur, 362, 428
Grün, E., Zook, H. A., Fechtig, H., & Giese, R. H. 1985, Icar, 62, 244
Gurnett, D. A., Grün, E., Gallagher, D., Kurth, W. S., & Scarf, F. L. 1983, Icar, 53, 236
Gurnett, D. A., Kurth, W. S., Kirchner, D. L., et al. 2004, SSRv, 114, 395
Hamilton, D. P., Grun, E., & Baghul, M. 1996, in ASP Conference Series, Vol. 104, Physics, Chemistry, and Dynamics of Interplanetary Dust, ed. B. A. S. Gustafson (San Francisco, CA: ASP), 31
Hsu, H.-W., Krüger, H., & Postberg, F. 2012, in Astrophysics and Space Science Library, Vol. 385, Nanodust in the Solar System: Discoveries and Interpretations (Berlin: Springer-Verlag), 77
Krimigis, S. M., Mitchell, D. G., Hamilton, D. C., et al. 2004, SSRv, 114, 233
Krüger, H., Graps, A. L., Hamilton, D. P., et al. 2006, P&SS, 54, 919
Küppers, M., O'Rourke, L., Bockelée-Morvan, D., et al. 2014, Natur, 505, 525
Li, A., & Mann, I. 2012, in Astrophysics and Space Science Library, Vol. 385, Nanodust in the Solar System: Discoveries and Interpretations (Berlin: Springer-Verlag), 5
Luhmann, J. G. 2003, P&SS, 51, 387
Mann, I., & Czechowski, A. 2012, in Astrophysics and Space Science Library, Vol. 385, Nanodust in the Solar System: Discoveries and Interpretations (Berlin: Springer-Verlag), 195
Mann, I., Meyer-Vernet, N., & Czechowski, A. 2014, PhR, 536, 1
Mann, I., Murad, E., & Czechowski, A. 2007, P&SS, 55, 1000
Maravilla, D., Flammer, K. R., & Mendis, D. A. 1995, ApJ, 438, 968
McBride, N., & McDonnell, J. A. M. 1999, P&SS, 47, 1005
Meyer-Vernet, N. 1979, JGR, 84, 5373
Meyer-Vernet, N. 1985, AdSpR, 5, 37
Meyer-Vernet, N., Lecacheux, A., Kaiser, M. L., & Gurnett, D. A. 2009a, GeoRL, 36, 3103
Meyer-Vernet, N., Lecacheux, A., & Pedersen, B. M. 1996, Icar, 123, 113
Meyer-Vernet, N., Maksimovic, M., Czechowski, A., et al. 2009b, SoPh, 256, 463
Meyer-Vernet, N., Mann, I., le Chat, G., et al. 2015, PPCF, 57, 014015
Meyer-Vernet, N., Moncuquet, M., Issautier, K., & Lecacheux, A. 2014, GeoRL, 41, 2716
Meyer-Vernet, N., & Perche, C. 1989, JGR, 94, 2405
Oberc, P. 1996, AdSpR, 17, 105
Schippers, P., Meyer-Vernet, N., Lecacheux, A., et al. 2014, GeoRL, 41, 5382
Spahn, F., Albers, N., Hörning, M., et al. 2006, P&SS, 54, 1024
Utterback, N. G., & Kissel, J. 1990, AJ, 100, 1315
Zaslavsky, A., Meyer-Vernet, N., Mann, I., et al. 2012, JGRA, 117, 5102
Zook, H. A., grün, E., Baguhl, M., et al. 1996, Sci, 274, 1501